Available online at www.sciencedirect.com
ScienceDirect
Trans. Nonferrous Met. Soc. China 33(2023) 1953−1962
Transactions of Nonferrous Metals Society of China
www.tnmsc.cn

A novel three-dimensional M-K model by integrating GTN model for accurately identifying limit strains of sheet metal

Yu-bao WANG, Cun-sheng ZHANG, Zi-jie MENG, Liang CHEN, Guo-qun ZHAO

Key Laboratory for Liquid−Solid Structural Evolution & Processing of Materials (Ministry of Education), Shandong University, Jinan 250061, China

Received 13 February 2022; accepted 2 June 2022

Abstract: To accurately identify the limit strains and improve the prediction accuracy of forming limits for sheet metal, a novel three-dimensional M-K model by integrating GTN model is developed and named 3D M-K-GTN model. By introducing the through-thickness normal stress and friction stress, the original M-K model is extended for adapting to the three-dimensional stress state. Furthermore, the empirical failure criterion is replaced by integrating the GTN model, and thus the limit strain is identified when the void volume fraction within the groove accumulates to a critical value. Besides, the voids nucleation and growth expressions are also re-derived and modified by embedding the friction stress and normal stress. Finally, the comparison between predicted forming limit curves and experimental limit strains of AA6016-T4 sheet indicates that the 3D M-K-GTN model solves the significant overestimation of prediction results under large strain paths, and always provides a high prediction accuracy for each strain path given.

Key words: limit strain identification; void evolution; failure criterion; 3D M-K-GTN model; prediction accuracy

1 Introduction

For predicting FLCs (forming limit curves) of sheet metals, the M-K (Marciniak−Kuczyński) model has been widely applied on account of its high accuracy and simple calculation form [1−4]. However, during the actual deformation process of sheet metals, the assumption of plane stress state for the original M-K model may be inapplicable when the material is in the three-dimensional stress condition [5−8]. Based on the modified M-K theory, MIRFALAH-NASIRI et al [9,10] have verified the effects of through-thickness normal and shear stresses on the forming limits. Besides, the modified M-K model by integrating friction stress and normal stress has also been established and proven to present a higher FLCs prediction accuracy for DP 600 and IF steels [11]. The accurate identification of material instability and failure in the calculation process significantly affects the FLCs prediction accuracy with the M-K model. MARCINIAK and KUCZYŃSKI [4] thought that the instability of material occurred when the strain in the uniform zone (ε^{a}) reached limit values. BARATA DA ROCHA et al [12] indicated that when the ratio of the equivalent strain increment in Zone a and b ($\mathrm{d}\overline{\varepsilon}^{b}/\mathrm{d}\overline{\varepsilon}^{a}$) was greater than 10, the limit strain was reached, but BANABIC et al [13] argued that the critical value should be 7. DING et al [14] found that there was little difference in the predicted FLCs with different critical values of $\mathrm{d}\overline{\varepsilon}^{b}/\mathrm{d}\overline{\varepsilon}^{a}$. At present, the commonly-used failure criterion is $\mathrm{d}\overline{\varepsilon}^{b}/\mathrm{d}\overline{\varepsilon}^{a} \geq 7$ or 10 when the M-K theory is used to predict the FLCs of sheet metals [15]. However, this criterion based on the difference of equivalent strain increment is very empirical and only reasonable when the necking phenomenon of material exists in the deformation process. For some materials with high

Corresponding author: Cun-sheng ZHANG, Tel: +86-15165138198, E-mail: zhangcs@sdu.edu.cn
DOI: 10.1016/S1003-6326(23)66235-1

specific strength, the fracture may occur before necking at the biaxial stretching state, which makes the predicted forming limits usually higher than the experimental results on the right hand of FLCs [16].

To accurately identify the failure of sheet metals, researchers have introduced various damage evolution mechanics models into M-K theory and proposed the so-called M-K-Damage models [17]. In these models, the initial inhomogeneity in materials can be realized by assuming that the defect area has a higher volume fraction of initial voids [18] and the limit strains are determined when the volume fraction of voids in the defect area reaches the critical value. KIM and KIM [19] proposed a modified M-K model with uniform void distribution to consider the influence of void evolution on the FLCs. It was found that the usual overestimation of limit strains at a biaxial stress state was significantly reduced by considering the void nucleation and growth phenomenon. ZADPOOR et al [20] studied the formability of high-strength aluminum alloy sheets with the Gurson porous plastic model, the M-K model and the M-K model coupling porous plastic model. Results indicated that only the coupling of M-K model and porous metal plastic model accurately predicted the FLCs within the whole range of stress triaxiality. Combining the Gurson model [21] proposed for porous plastic materials with M-K model, NEEDLEMAN and TRIANTAFYLLIDIS [22] studied the influence of void growth on the local necking in biaxial tensile sheets. Besides, CHU and NEEDLEMAN [23] found that the nucleation parameters of new voids directly affected the shape of predicted FLCs. By simultaneously considering the nucleation of particles and the growth of voids, a prediction method of forming limits for sheet metals was proposed by MELANDER [24] with the coupling of different porous plastic damage models and the M-K model. HUANG et al [25] and CHIEN et al [26] introduced the improved macroscopic anisotropy Gurson model into the M-K model and studied the influence of initial void volume fraction and anisotropy coefficient on predicting FLCs. HOSSEINI et al [27] accurately predicted the FLCs of AK and IF steels by employing the M-K-Gurson model with a geometrical groove and unevenly-distributed initial voids. In the finite element simulation of Nakazima tests, the GTN model was introduced for determining the FLCs of sheet metals by KAMI et al [28], and it was concluded that the employment of GTN model was an effective method to improve the prediction accuracy of forming limits in the biaxial tension state. LIU et al [29] combined the GTN model with the numerical M-K model and concluded that the accurate prediction of FLCs could be obtained when the volume fraction of initial void was set as 0.007 for the AA6111-T4 sheet.

From the above analysis, the M-K model combined with the porous plastic damage models could provide a good FLCs prediction of sheet metals, but little work has been reported on the integration of advanced GTN damage model in the 3D M-K model. Thus, in this work, a novel 3D M-K model by integrating GTN model is developed. Furthermore, the comparison between experimental forming limits of AA6016-T4 sheet and predicted FLCs is performed for evaluating the validity of this 3D M-K-GTN model.

2 Establishment of 3D M-K-GTN model

2.1 Three-dimensional (3D) M-K model

To establish the 3D M-K model, the three-dimensional stress state of the specimens during Nakazima test is analyzed. Figure 1 demonstrates the diagram of the selected force body, which is near the apex of the specimen. Equation (1) shows the expression of the normal stress that is proposed in the previous work by establishing the force equilibrium equation along the thickness direction and considering the stress gradient [11]:

$$\sigma_R = \frac{2t}{R}(\sigma_\theta + P\sigma_\varphi) \tag{1}$$

where R denotes the punch radius, t is the thickness of sheet metal, P $(=[\mathrm{d}\beta/(\sin\theta \mathrm{d}\varphi)])$ indicates the specimen failure position, the radians θ and φ define the location of force body.

Besides the through-thickness normal stress, friction exists on the contact surface during the deformation process of the specimens, which has a non-negligible effect on the limit strains. Based on the stress state and geometrical shape of force body, the friction force (f') is defined, as given in Eq. (2). However, the M-K model cannot directly consider the shear force induced by friction. Thus, the shear force is equivalent to the stress increment along the major stress direction in the M-K model. This

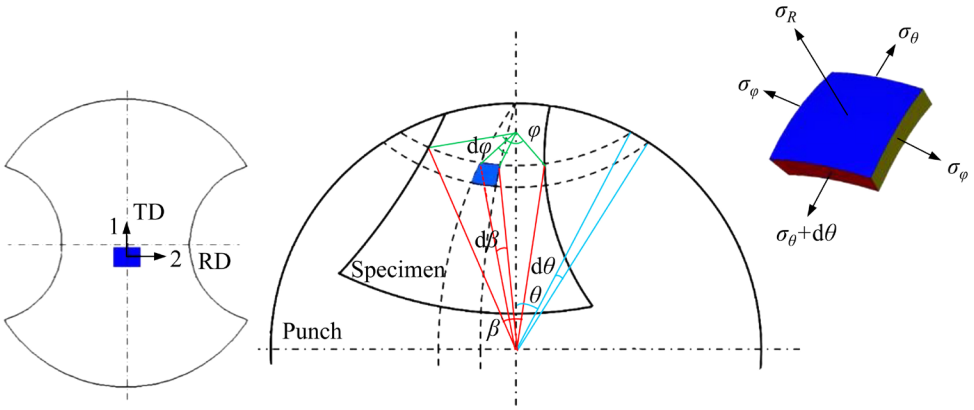

Fig. 1 Diagram of selected force body [11]

friction stress is denoted as σ_f and defined by Eq. (3):

$$f'=\mu\sigma_R S_R \tag{2}$$

$$\sigma_f = 2\mu d\theta(\sigma_1 + P\sigma_2) \tag{3}$$

where μ indicates the friction coefficient, S_R denotes the contact area and dθ defines the size of the force body.

On this basis, the 3D M-K model which describes the three-dimensional stress state of sheet metals is established, as shown in Fig. 2. In comparison with the original M-K model, the major stress is extended by adding the friction stress component and the normal stress is introduced.

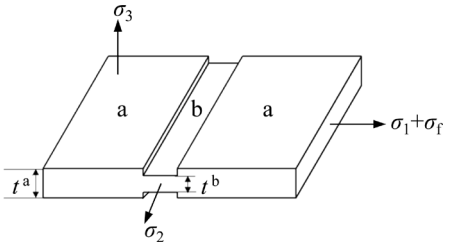

Fig. 2 Schematic diagram of 3D M-K model

2.2 Employment of GTN damage model

During the plastic deformation process of sheet metals, defects such as micro-voids usually exist inside the materials [30,31]. The evolution process of the voids includes the nucleation, growth and coalescence stages [32]. The damage evolution models can describe the physical characteristics of ductile fracture caused by the accumulation of internal damage [33]. Then, the yield criterion that simultaneously considers the voids nucleation and growth in the porous plastic materials is proposed, as given in Eq. (4). It takes the void volume fraction (f) as the damage variable, which can reflect the influence of damage evolution on the macroscopic mechanical properties of the materials:

$$\Phi = \left(\frac{\sigma_{eq}}{\bar{\sigma}_M}\right)^2 + 2f\cosh\left(-\frac{3\sigma_h}{2\bar{\sigma}_M}\right) - (1+f^2) = 0 \tag{4}$$

where $\bar{\sigma}_M$ donotes the equivalent stress of the matrix material and σ_h indicates the hydrostatic stress.

Later, to consider the load-carrying capacity loss of materials resulting from the void interaction and void coalescence during deformation, the above Gurson model was extended by introducing three new material parameters q_1, q_2 and q_3 [23,34−36]. Consequently, the widely used Gurson−Tvergaard−Needleman (GTN) model [37] was established as

$$\Phi = \left(\frac{\sigma_{eq}}{\bar{\sigma}_M}\right)^2 + 2fq_1\cosh\left(-\frac{3q_2\sigma_h}{2\bar{\sigma}_M}\right) - (1+q_3f^2) = 0 \tag{5}$$

In this work, for accurately identifying the failure of sheet metals and determining the corresponding forming limits, the damage evolution mechanical model is integrated into the 3D M-K model by assuming that the initial voids exist, as presented in Fig. 3. It is supposed that besides the initial thickness imperfection ($g_0 = t_0^b/t_0^a$) of the M-K model, a higher volume fraction of initial voids (f_0^b) exists in the groove. During the deformation process, the voids growth and the nucleation of new voids at the second phase particles and inclusions in the material are described by the GTN model. Meanwhile, the failure of materials occurs when the volume fraction of voids in Zone b (f^b) reaches the critical

value of void volume fraction (f_c). Hence, the GTN model and the 3D M-K model are successfully combined and named the 3D M-K-GTN model.

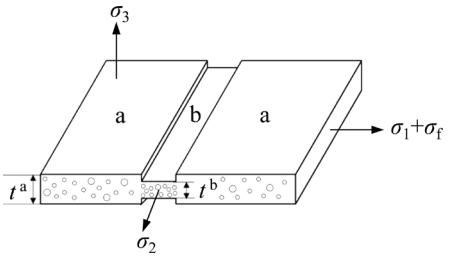

Fig. 3 Diagram of 3D M-K model with initial voids

When considering the three-dimensional stress state of the 3D M-K model, the hydrostatic pressure (σ_h) in the GTN model is defined by the following equation:

$$\sigma_h = \frac{\sigma_1' + \sigma_2 + \sigma_3}{3} \tag{6}$$

where the expression of normal stress is defined in Eq. (7) by applying the principal stress components in Eq. (1) and Eq. (8) presents the introduction of friction stress:

$$\sigma_3 = \frac{2t}{R}\left(\sigma_1 + P\sigma_2\right) \tag{7}$$

$$\sigma_1' = \sigma_1 + \sigma_f \tag{8}$$

The isotropic von Mises yield criterion as shown in Eq. (9) describes the yield behavior of materials in the original GTN model:

$$\bar{\sigma}^2 = \sigma_1^2 + \sigma_2^2 + \sigma_3^2 - \sigma_1\sigma_2 \tag{9}$$

By considering the anisotropy of sheet metals, the anisotropic Hill's 48 yield criterion is used in the GTN model and its expression is also modified, as shown in Eq. (10), based on the stress state of the 3D M-K model:

$$\bar{\sigma}^2 = F(\sigma_2 - \sigma_3)^2 + G(\sigma_3 - \sigma_1 - \sigma_f)^2 + H(\sigma_1 + \sigma_f - \sigma_2)^2 \tag{10}$$

Moreover, the hyperbolic cosine term involved in the GTN damage model makes the further forming limits calculation more difficult within the M-K model framework. Therefore, the Taylor series is applied to expanding the hyperbolic cosine and the items with a power higher than 2 are disregarded [38]. As a result, the following form of GTN model is obtained and used in this work:

$$\Phi = \left(\frac{\bar{\sigma}}{\bar{\sigma}_M}\right)^2 + 2fq_1\left(1 + \frac{1}{2}\left(\frac{3q_2\sigma_h}{2\bar{\sigma}_M}\right)^2\right) - (1 + q_3f^2) = 0 \tag{11}$$

3 FLCs prediction with 3D M-K-GTN model

During the plastic deformation process of sheet metals, the relation between stress and increments of strain follows the Levy−Mises flow rule:

$$d\varepsilon_i = d\lambda\frac{\partial\Phi}{\partial\sigma_i} \quad (i=1,\ 2,\ 3) \tag{12}$$

where $d\varepsilon_i$ denotes the increment of strain components, $d\lambda$ is a non-negative proportionality coefficient and i indicates the direction. Moreover, the equivalent stress is defined by the GTN model expressed in Eq. (11), in which the modified expressions of hydrostatic pressure and Hill's 48 yield function as shown in Eqs. (6) and (10) are used. Thus, the increments of strain components along different directions are obtained as

$$\begin{cases} d\varepsilon_1 = \dfrac{d\lambda}{(\bar{\sigma}_M)^2}[2G(\sigma_1 + \sigma_f - \sigma_3) + 2H(\sigma_1 + \sigma_f - \sigma_2) + 1/2fq_1q_2^2(\sigma_1 + \sigma_f + \sigma_2 + \sigma_3)] \\ d\varepsilon_2 = \dfrac{d\lambda}{(\bar{\sigma}_M)^2}[2F(\sigma_2 - \sigma_3) + 2H(\sigma_2 - \sigma_1 - \sigma_f) + 1/2fq_1q_2^2(\sigma_1 + \sigma_f + \sigma_2 + \sigma_3)] \\ d\varepsilon_3 = \dfrac{d\lambda}{(\bar{\sigma}_M)^2}[2F(\sigma_3 - \sigma_2) + 2G(\sigma_3 - \sigma_1 - \sigma_f) + 1/2fq_1q_2^2(\sigma_1 + \sigma_f + \sigma_2 + \sigma_3)] \end{cases} \tag{13}$$

where $\bar{\sigma}_M$ denotes the equivalent stress of the matrix material.

Considering the voids evolution during the deformation process, the volume strain increment ($d\varepsilon_V$) of the macroscopic material is expressed by Eq. (14) and the volume of the matrix material (V_M) is defined by Eq. (15):

$$d\varepsilon_V = d\varepsilon_1 + d\varepsilon_2 + d\varepsilon_3 = 3/2d\lambda fq_1q_2^2(\sigma_1 + \sigma_f + \sigma_2 + \sigma_3)/\bar{\sigma}_M^2 \tag{14}$$

$$V_M = V - V_f = V(1-f) \tag{15}$$

where V and V_f respectively denote the volumes of

macroscopic material and voids.

Then, by taking differentiation for each side of Eq. (15) and considering the incompressibility of matrix material, the relation between increments of macroscopic material volume and volume fraction of void is obtained as

$$\frac{\mathrm{d}V}{V}=\frac{\mathrm{d}f}{1-f} \tag{16}$$

This means

$$\mathrm{d}\varepsilon_V=\frac{\mathrm{d}V}{V}=\frac{\mathrm{d}f}{1-f} \tag{17}$$

By combining Eqs. (14) and (17), the non-negative proportionality coefficient $\mathrm{d}\lambda$ is expressed as

$$\mathrm{d}\lambda=\frac{2\mathrm{d}f\,\bar{\sigma}_{\mathrm{M}}^2}{3fq_1q_2^2(\sigma_1+\sigma_f+\sigma_2+\sigma_3)(1-f)} \tag{18}$$

Afterward, through substituting the above expression of $\mathrm{d}\lambda$ (Eq. (18)) into Eq. (13), the increment of the major strain is defined by the following equation:

$$\begin{aligned}\mathrm{d}\varepsilon_1=\{&2\mathrm{d}f[2G(\sigma_1+\sigma_{\mathrm{f}}-\sigma_3)+2H(\sigma_1+\sigma_{\mathrm{f}}-\sigma_2)+\\&1/2fq_1q_2^2(\sigma_1+\sigma_{\mathrm{f}}+\sigma_2+\sigma_3)]\}/\\&[3fq_1q_2^2(\sigma_1+\sigma_{\mathrm{f}}+\sigma_2+\sigma_3)(1-f)]\end{aligned} \tag{19}$$

Moreover, the expression of the void volume fraction increment in deformation process is obtained as shown in Eq. (20) by transforming the above formula. It is found that the increment of void volume fraction is decided by the current void volume fraction (f), the stress components and the increment of major strain:

$$\begin{aligned}\mathrm{d}f=\{&[3fq_1q_2^2(\sigma_1+\sigma_{\mathrm{f}}+\sigma_2+\sigma_3)(1-f)]/\\&[4G(\sigma_1+\sigma_{\mathrm{f}}-\sigma_3)+4H(\sigma_1+\sigma_{\mathrm{f}}-\sigma_2)+\\&2fq_1q_2^2(\sigma_1+\sigma_{\mathrm{f}}+\sigma_2+\sigma_3)]\}\mathrm{d}\varepsilon_1\end{aligned} \tag{20}$$

During the deformation process of the sheet metals, besides the growth of existing voids, the evolution of void damage includes the nucleation of new voids. Thus, the increment of the void volume fraction should incorporate the increments respectively induced by voids growth and nucleation of new voids. Based on the analysis of CHU and NEEDLEMAN [23], the void nucleation is controlled by the equivalent strain increment of matrix material, as given in Eq. (21):

$$\mathrm{d}f_{\mathrm{nucleation}}=A_{\mathrm{N}}\mathrm{d}\bar{\varepsilon}_{\mathrm{M}} \tag{21}$$

$$A_{\mathrm{N}}=\frac{f_{\mathrm{N}}}{S_{\mathrm{N}}\sqrt{2\pi}}\left[-\frac{1}{2}\left(\frac{\bar{\varepsilon}_{\mathrm{M}}-\varepsilon_{\mathrm{N}}}{S_{\mathrm{N}}}\right)^2\right] \tag{22}$$

where f_{N}, ε_{N} and S_{N} are material parameters.

For calculating the increment of equivalent strain for the matrix material, Eq. (23) is established based on the equality relationship of plastic work between the macroscopic material and the matrix material:

$$\sigma_1\mathrm{d}\varepsilon_1+\sigma_2\mathrm{d}\varepsilon_2+\sigma_3\mathrm{d}\varepsilon_3=\bar{\sigma}_{\mathrm{M}}\mathrm{d}\bar{\varepsilon}_{\mathrm{M}}(1-f) \tag{23}$$

The equivalent stress of the matrix material is obtained by the following equation:

$$\bar{\sigma}_{\mathrm{M}}=\frac{1}{1-fq_1}\sqrt{\bar{\sigma}^2+\frac{9}{4}q_1q_2^2\sigma_{\mathrm{h}}^2} \tag{24}$$

where the equivalent stress is defined by the Swift model as given in Eq. (25) and the parameters K, n and ε_0 in this hardening model respectively denote the hardening coefficient, the hardening index and the pre-strain [39,40].

$$\bar{\sigma}=K(\varepsilon_0+\bar{\varepsilon}^{\mathrm{p}})^n \tag{25}$$

In the 3D M-K-GTN model, the compatibility equation of deformation and the equation of force equilibrium respectively as given in Eq. (26) and Eq. (27) are still available according to the basic assumption of M-K theory. But different from the original M-K model, it is supposed that the initial imperfection in the 3D M-K-GTN model is realized by the combination of thickness reduction and a higher void volume fraction inside the groove. Besides, by considering that the external load of the material with voids is all supported by the matrix material, the force equilibrium equation is modified in form of Eq. (28). Furthermore, by substituting Eq. (25), the relationship between the volume fraction of voids and the strains during the deformation process of the materials is obtained, as given in Eq. (29):

$$\mathrm{d}\varepsilon_2^{\mathrm{a}}=\mathrm{d}\varepsilon_2^{\mathrm{b}} \tag{26}$$

$$\sigma_1^{\mathrm{a}}t^{\mathrm{a}}=\sigma_1^{\mathrm{b}}t^{\mathrm{b}} \tag{27}$$

$$\sigma_{\mathrm{M}}^{\mathrm{a}}t^{\mathrm{a}}(1-f^{\mathrm{a}})=\sigma_{\mathrm{M}}^{\mathrm{b}}t^{\mathrm{b}}(1-f^{\mathrm{b}}) \tag{28}$$

$$\frac{(\varepsilon_0+\bar{\varepsilon}_{\mathrm{M}}^{\mathrm{a}})^n}{\varphi_{\mathrm{M}}^{\mathrm{a}}}t^{\mathrm{a}}(1-f^{\mathrm{a}})=\frac{(\varepsilon_0+\bar{\varepsilon}_{\mathrm{M}}^{\mathrm{b}})^n}{\varphi_{\mathrm{M}}^{\mathrm{b}}}t^{\mathrm{b}}(1-f^{\mathrm{b}}) \quad (29)$$

where $\varphi_{\mathrm{M}}^{\mathrm{a}}$ and $\varphi_{\mathrm{M}}^{\mathrm{b}}$ denote the ratios of equivalent stress to major stress of the matrix materials respectively in Zones a and b.

Figure 4 demonstrates the FLCs prediction process with the 3D M-K-GTN model. Firstly, the required parameters in the 3D M-K-GTN model and the materials coefficients are given at the beginning of the calculation. Secondly, the increments of strain components and the increment of void volume fraction in Zone a are obtained. Then, through solving Eq. (29) with the numerical iteration method, the increments of strain components and the void volume fraction in Zone b are calculated. Afterward, the calculation process is repeated and the corresponding results are updated until the instability criterion that the accumulation of void volume fraction in Zone b reaches the critical value ($f^{\mathrm{b}}\geq f_{\mathrm{c}}$) is satisfied. At last, the minor and major strains in Zone a updated at the material failure moment are taken as the limit strains. Furthermore, the above process is repeated in the loop of the stress ratio to determine the whole FLCs.

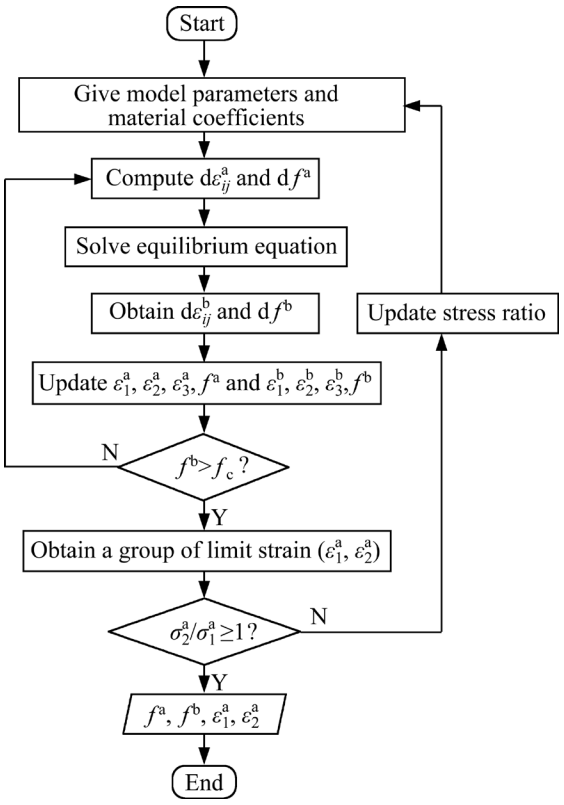

Fig. 4 FLCs prediction process with 3D M-K-GTN model

4 Validation of 3D M-K-GTN model

To evaluate the validity of the 3D M-K-GTN model, the FLCs of the AA6016-T4 sheet are predicted by introducing the required material parameters into the calculation program developed in Section 3, and then compared with the Nakazima test results. Besides, the predicted FLCs of the original M-K model and the 3D M-K model proposed by WANG et al [11] are obtained and compared. For the AA 6016-T4 sheet, Table 1 lists its hardening and anisotropy materials parameters and Table 2 gives material parameters in the GTN model. Meanwhile, five groups of limit strains of the sheet at the strain paths of −0.32, 0.07, 0.18, 0.32 and 0.82 are obtained by picking up the experimental results from the literature [28] and used for the present comparison.

Table 1 Hardening and anisotropy material parameters of AA6016-T4 sheet [28]

Swift hardening model			Hill's 48 yield criterion		
K	n	ε_0	F	G	H
525.77	0.2704	0.011252	0.648	0.644	0.356

Table 2 Material parameters of AA6016-T4 sheet in GTN model [28]

q_1	q_2	q_3	f_0	f_c	f_0	ε_N	S_N
1.5	1	2.25	0.00035	0.05	0.05	0.3	0.1

Besides the materials parameters listed in Tables 1 and 2, the initial void volume fraction inside the groove (f_0^{b}) and the initial thickness imperfection (g_0), which are supposed in the 3D M-K-GTN model, have a significant influence on the prediction accuracy of FLCs. Thus, the experimental forming limit at the strain path of −0.32 is taken as the standard to determine the supposed parameters (f_0^{b} and g_0). Here, after several examinations, one combination of the supposed parameters (g_0=0.99, f_0^{b}=0.0004) in the 3D M-K-GTN model is determined and Fig. 5 shows the change of the void volume fraction in Zone a and Zone b during the calculation process with these parameters. It can be found that when the calculated major strain approaches the experimental limit major strain ($\varepsilon_{\mathrm{Exp}}^{*}$), the void volume fraction in Zone b (f^{b}) approximatively attains the critical

void volume fraction (f_c), which indicates that the initial void volume fraction inside the groove (f_0^b) of 0.0004 and the initial thickness imperfection (g_0) of 0.99 used in the 3D M-K-GTN model are reasonable. However, for the 3D M-K model with the initial thickness imperfection (g_0) of 0.945, when the specific value of increments of equivalent strain in Zones a and b ($d\bar{\varepsilon}^b/d\bar{\varepsilon}^a$) reaches the empirical failure value of 10, the predicted major strain is close to the limit strain ($\varepsilon^*_{Exp.}$) as shown in Fig. 5. Thus, the applied initial thickness imperfection (g_0) of 0.945 is valid in the 3D M-K model.

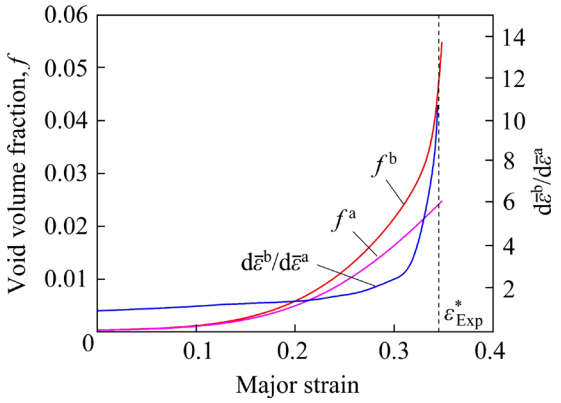

Fig. 5 Evolution of void volume fraction and specific value ($d\bar{\varepsilon}^b/d\bar{\varepsilon}^a$) at strain path of −0.32

With the determined parameters (f_0^b and g_0), the complete FLCs are predicted based on different M-K models and Fig. 6 presents their comparison with the experimental results. It is found that on the left side and within the range of small strain paths, the three predicted forming limit curves present a similar change trend, and they are very close to the experimental ones. However, it can be clearly noted that with the strain path continuously increasing, the predicted FLCs of the original M-K model and the 3D M-K model present a monotonous increasing trend while the rightmost test point ends at a relatively low level, which makes the predicted values of these two M-K models much higher than the experimental limit major strains. Fortunately, the FLCs predicted by the 3D M-K-GTN model present a declining trend with the strain ratio approaching the equi-biaxial stretching state, which makes the predicted data closer to the Nakazima test results and leads to an improvement in the forming limits prediction accuracy under large strain paths.

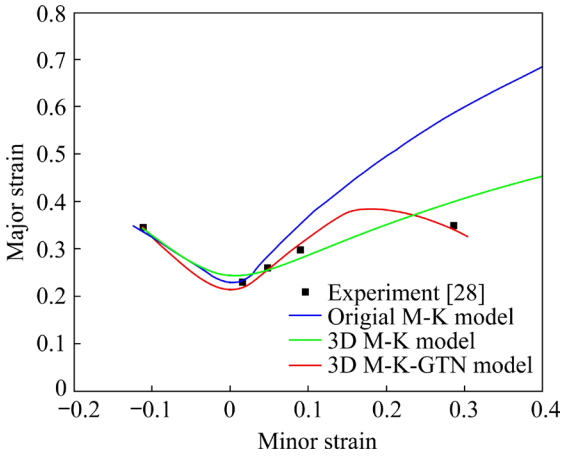

Fig. 6 FLCs predicted with different M-K models and obtained by Nakazima tests

To further quantify the prediction accuracy of FLCs with the 3D M-K model and the 3D M-K-GTN model, the predicted limit major strains and the corresponding prediction errors under different experimental strain paths are obtained and listed in Table 3. Here, ε^*_{10} denotes the predicted major strain of the 3D M-K model with the empirical failure criterion ($d\bar{\varepsilon}^b/d\bar{\varepsilon}^a \geq 10$), and ε^*_{GTN} indicates the limit major strain in the 3D M-K-GTN model obtained when the failure criterion of void accumulation is satisfied ($f^b \geq f_c$). It can be found from Table 3 that when the strain path is 0.07, 0.18, and 0.32, the 3D M-K model gives the corresponding errors of 6.3%, 1.7% and 7.4%, and the prediction errors of the 3D M-K-GTN model are 5.2%, 0.77% and 5.7%, respectively. Especially, under the large strain path of 0.82, the predicted strain of the 3D M-K-GTN agrees extremely well with the experimental one, which gives an error of 1.7%, while the prediction error of the 3D M-K model is 24.9%. Therefore, it can be concluded that the 3D M-K-GTN model

Table 3 Limit major strains obtained by different M-K models and prediction errors

Strain path	ε^*_{Exp}	3D M-K model		3D M-K-GTN model	
		ε^*_{10}	Error/%	ε^*_{GTN}	Error/%
−0.32	0.345	0.343	–	0.347	–
0.07	0.23	0.2445	6.3	0.218	5.2
0.18	0.26	0.2556	1.7	0.258	0.77
0.32	0.298	0.276	7.4	0.315	5.7
0.82	0.349	0.4358	24.9	0.343	1.7

always provides a higher prediction accuracy than the 3D M-K model for each strain path given. In addition, it can be noted that at the strain path of 0.18, the errors for both predicted results are very small. This is because there exist some ranges of strain path, where different predicted curves would be very close to experimental points and even coincide at a certain value.

The 3D M-K-GTN model could solve the usual overestimation of predicted limit strains under biaxial stretching state commonly reported in the current literature [41]. To investigate this phenomenon, the changes of the void volume fraction in Zones a and b during the 3D M-K-GTN calculation process at the strain path of 0.82 are presented in Fig. 7. Besides, the specific value ($\mathrm{d}\bar{\varepsilon}^{\mathrm{b}}/\mathrm{d}\bar{\varepsilon}^{\mathrm{a}}$) in the 3D M-K model is also plotted. It can be found that as the deformation proceeds, the accumulation speeds of void volume fraction in Zone a and Zone b have little difference. Similarly, the specific value ($\mathrm{d}\bar{\varepsilon}^{\mathrm{b}}/\mathrm{d}\bar{\varepsilon}^{\mathrm{a}}$) keeps at a low level before the experimental limit strain ($\varepsilon^{*}_{\mathrm{Exp}}$) is attained, which indicates that the fracture of material occurs before necking at the biaxial stretching state. Therefore, within the range of large strain path, the M-K model that uses the empirical failure criterion ($\mathrm{d}\bar{\varepsilon}^{\mathrm{b}}/\mathrm{d}\bar{\varepsilon}^{\mathrm{a}} \geq 10$) based on the necking phenomenon is not suitable. On the contrary, the critical void volume fraction (f_{c}) is attained almost simultaneously with the moment when the calculated strain with the 3D M-K-GTN model reaches the experimental limit strain ($\varepsilon^{*}_{\mathrm{Exp}}$). Consequently, the 3D M-K-GTN model always presents a high FLCs prediction accuracy within the entire range of strain path.

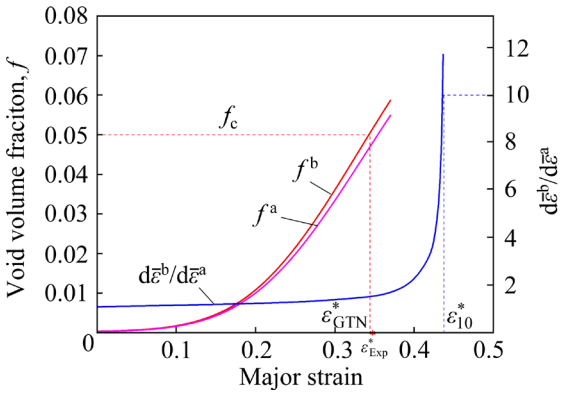

Fig. 7 Evolution of void volume fraction and specific value ($\mathrm{d}\bar{\varepsilon}^{\mathrm{b}}/\mathrm{d}\bar{\varepsilon}^{\mathrm{a}}$) at strain path of 0.82

5 Conclusions

(1) On the left side of the FLCs or under small strain paths, the predicted FLCs with different M-K models present a similar change trend and approximate to the experimental limit strains. Therefore, it is concluded that all the classical M-K model, the 3D M-K model and the 3D M-K-GTN model are reliable within this range.

(2) With the deformation of the materials approaching the equi-biaxial stress state, the limit major strains calculated by the 3D M-K model and the original M-K model are both overestimated, and only the developed 3D M-K-GTN model keeps in a high FLCs prediction accuracy. This difference is explained by the phenomenon that the failure of sheet metals occurs before necking under large strain paths, which makes the empirical failure criterion ($\mathrm{d}\bar{\varepsilon}^{\mathrm{b}}/\mathrm{d}\bar{\varepsilon}^{\mathrm{a}} \geq 10$) unreasonable, but the damage-based identification ($f^{\mathrm{b}} \geq f_{\mathrm{c}}$) in the 3D M-K-GTN model is unaffected. As a result, it is suggested that the material failure during the deformation process should be identified based on the damage accumulation when predicting the FLCs with M-K model.

Acknowledgments

This work was supported by the National Natural Science Foundation of China (No. 51975330), Key Research and Development Program of Shandong Province, China (No. 2021ZLGX01), and Project of Colleges and Universities Innovation Team of Jinan City, China (No. 2021GXRC030).

References

[1] LI Zi-han, ZHOU Guo-wei, LI Da-yong, JAIN M K, PENG Ying-hong, WU Pei-dong. Forming limits of magnesium alloy AZ31B sheet at elevated temperatures [J]. International Journal of Plasticity, 2020, 135: 102822.

[2] DONG Guo-jiang, CHEN Zhi-wei, YANG Zhuo-yun, FAN Bo-cheng. Comparative study on forming limit prediction of AA7075-T6 sheet with M-K model and Lou−Huh criterion [J]. Transactions of Nonferrous Metals Society of China, 2020, 30: 1463−1477.

[3] LI Xiao-qiang, DONG Hong-rui, WANG Hai-bo, GUO Gui-qiang, LI Dong-sheng. Effect of strain rate difference between inside and outside groove in M-K model on prediction of forming limit curve of Ti6Al4V at elevated temperatures [J]. Transactions of Nonferrous Metals Society

of China, 2020, 30: 405−416.

[4] MARCINIAK Z, KUCZYŃSKI K. Limit strains in the processes of stretch-forming sheet metal [J]. International Journal of Mechanical Sciences, 1967, 9: 609−620.

[5] MA B L, WAN M, CAI Z Y, YUAN W N, LI C, WU X D, LIU W. Investigation on the forming limits of 5754-O aluminum alloy sheet with the numerical Marciniak−Kuczyński approach [J]. International Journal of Mechanical Sciences, 2018, 142/143: 420−431.

[6] HU Qi, LI Xi-feng, CHEN Jun. Forming limit evaluation by considering through-thickness normal stress: Theory and modeling [J]. International Journal of Mechanical Sciences, 2019, 155: 187−196.

[7] MORCHHALE A, BADRISH A, KOTKUNDE N, SINGH S K, KHANNA N, SAXENA A, NIKHARE C. Prediction of fracture limits of Ni−Cr based alloy under warm forming condition using ductile damage models and numerical method [J]. Transactions of Nonferrous Metals Society of China, 2021, 31: 2372−2387.

[8] WU P D, EMBURY J D, LLOYD D J, HUANG Y, NEALE K W. Effects of superimposed hydrostatic pressure on sheet metal formability [J]. International Journal of Plasticity, 2009, 25: 1711−1725.

[9] MIRFALAH-NASIRI S M, BASTI A, HASHEMI R. Forming limit curves analysis of aluminum alloy considering the through-thickness normal stress, anisotropic yield functions and strain rate [J]. International Journal of Mechanical Sciences, 2016, 117: 93−101.

[10] MIRFALAH-NASIRI S M, BASTI A, HASHEMI R, DARVIZEH A. Effects of normal and through-thickness shear stresses on the forming limit curves of AA3104-H19 using advanced yield criteria [J]. International Journal of Mechanical Sciences, 2018, 137: 15−23.

[11] WANG Yu-bao, ZHANG Cun-sheng, YANG Ying, FAN Shu-ming, WANG Guang-chun, ZHAO Guo-qun, CHEN Liang. The integration of through-thickness normal stress and friction stress in the M-K model to improve the accuracy of predicted FLCs [J]. International Journal of Plasticity, 2019, 120: 147−163.

[12] da ROCHA A B, BARLAT F, JALINIER J M. Prediction of the forming limit diagrams of anisotropic sheets in linear and non-linear loading [J]. Materials Science and Engineering, 1985, 68: 151−164.

[13] BANABIC D, COMSA S, JURCO P, COSOVICI G, PARAIANU L, JULEAN D. FLD theoretical model using a new anisotropic yield criterion [J]. Journal of Materials Processing Technology, 2004, 157/158: 23−27.

[14] DING Jie, ZHANG Cun-sheng, CHU Xing-rong, ZHAO Guo-qun, LEOTOING L, GUINES D. Investigation of the influence of the initial groove angle in the M-K model on limit strains and forming limit curves [J]. International Journal of Mechanical Sciences, 2015, 98: 59−69.

[15] ZHANG Rui-qiang, SHAO Zhu-tao, LIN Jian-guo. A review on modelling techniques for formability prediction of sheet metal forming [J]. International Journal of Lightweight Materials and Manufacture, 2018, 1: 115−125.

[16] MU Lei, JIA Zhe, MA Zi-wei, SHEN Fu-hui, SUN Yue-kuo, ZANG Yong. A theoretical prediction framework for the construction of a fracture forming limit curve accounting for fracture pattern transition [J]. International Journal of Plasticity, 2020, 129: 102706.

[17] BANABIC D, KAMI A, COMSA D S, EYCKENS P. Developments of the Marciniak−Kuczyński model for sheet metal formability: A review [J]. Journal of Materials Processing Technology, 2021, 287: 116446.

[18] GOLOGANU M, COMSA D S, BANABIC D. Theoretical model for forming limit diagram predictions without initial inhomogeneity [J]. AIP Conference Proceeding, 2013, 1532: 245−253.

[19] KIM K H, KIM D W. The effect of void growth on the limit strains of steel sheets [J]. International Journal of Mechanical Sciences, 1983, 25: 293−300.

[20] ZADPOOR A A, SINKE J, BENEDICTUS R. Formability prediction of high strength aluminum sheets [J]. International Journal of Plasticity, 2009, 25: 2269−2297.

[21] GURSON A L. Continuum theory of ductile rupture by void nucleation and growth. Part I: Yield criteria and flow rules for porous ductile media [J]. Journal of Engineering and Materials and Technology, 1977, 99: 2−15.

[22] NEEDLEMAN A. TRIANTAFYLLIDIS N. Void growth and local necking in biaxially stretched sheets [J]. Journal of Engineering Materials, 1978, 100: 164−169.

[23] CHU C C, NEEDLEMAN A. Void nucleation effects in biaxially stretched sheets [J]. Journal of Engineering Materials and Technology, 1980, 102: 249−256.

[24] MELANDER A. A new model of the forming limit diagram applied to experiments on four copper-base alloys [J]. Materials Science and Engineering, 1983, 58: 63−88.

[25] HUANG H M, PAN J, TANG S C. Failure prediction in anisotropic sheet metals under forming operations with consideration of rotating principal stretch directions [J]. International Journal of Plasticity, 2000, 16: 611−633.

[26] CHIEN W Y, PAN J, TANG S C. A combined necking and shear localization analysis for aluminum sheets under biaxial stretching conditions [J]. International Journal of Plasticity, 2004, 20: 1953−1981.

[27] HOSSEINI M E, HOSSEINIPOUR S J, BAKHSHI-JOOYBARI M. Theoretical FLD prediction based on M-K model using Gurson's plastic potential function for steel sheets [J]. Procedia Engineering, 2017, 183: 119−124.

[28] KAMI A, DARIANI B M, VANINI A S, COMSA D S. Numerical determination of the forming limit curves of anisotropic sheet metals using GTN damage model [J]. Journal of Materials Processing Technology, 2015, 216: 472−483.

[29] LIU Jian-guang, WANG Zhong-jin, MENG Qing-yuan. Numerical investigations on the influence of superimposed double-sided pressure on the formability of biaxially stretched AA6111-T4 sheet metal [J]. Journal of Materials Engineering and Performance, 2012, 21: 429−436.

[30] ROUSSELIER G. Porous plasticity revisited: Macroscopic and multiscale modeling [J]. International Journal of Plasticity, 2020, 136: 102881.

[31] LI Kai-di, HAN Xiao-ning, TANG Bin, ZHANG Meng-qi, LI Jin-shan. Effect of microvoids on microplasticity behavior of dual-phase titanium alloy under high cyclic loading (I): Crystal plasticity analysis [J]. Transactions of Nonferrous Metals Society of China, 2022, 32: 513−523.

[32] MALCHER L, ANDRADE PIRES F M, CÉSÁR DE SA J M A. An extended GTN model for ductile fracture under high and low stress triaxiality [J]. International Journal of Plasticity, 2014, 54: 193−228.
[33] CHEN You-bin, LORENTZ E, BESSON J. Crack initiation and propagation in small-scale yielding using a nonlocal GTN model [J]. International Journal of Plasticity, 2020, 130: 102701.
[34] TVERGAAD V. On localization in ductile materials containing spherical voids [J]. International Journal of Fracture, 1982, 18: 237−252.
[35] TVERGAAD V. Influence of void nucleation on ductile shear fracture at a free surface [J]. Journal of the Mechanics and Physics of Solids, 1982, 30: 399−425.
[36] TVERGAAD V, NEEDLEMAN A. Analysis of the cup-cone fracture in a round tensile bar [J]. Acta Metallurgica, 1984, 32: 157−169.
[37] PARK N, STOUGHTON T B, YOON J W. A new approach for fracture prediction considering general anisotropy of metal sheets [J]. International Journal of Plasticity, 2020, 124: 199−225.
[38] RAGAB A R, SALEH C A R. Evaluation of constitutive models for voided solids [J]. International Journal of Plasticity, 1999, 15: 1041−1065.
[39] SAFIKHANI A R, HASHEMI R, ASSEMPOUR A. The strain gradient approach for determination of forming limit stress and strain diagrams [J]. Proceedings of the Institution of Mechanical Engineers, Part B: Journal of Engineering Manufacture, 2008, 222: 467−483.
[40] JIAO Zhi-hui, LANG Li-hui, ZHAO Xiang-ni. 5A06-O aluminium-magnesium alloy sheet warm hydroforming and optimization of process parameters [J]. Transactions of Nonferrous Metals Society of China, 2021, 31: 2939−2948.
[41] CHEN Liang-yu, FANG Su-ping, ZHAO Kun-min, XIAO Rui, ZHAI Hua. Forming limit prediction using an integrated model for 7075 aluminum alloy sheets at an elevated temperature [J]. International Journal of Solids and Structures, 2020, 202: 475−485.

一种新的耦合 GTN 模型以精确识别金属板料极限应变的三维 M-K 模型

王玉宝，张存生，孟子杰，陈 良，赵国群

山东大学 材料液固结构演变与加工教育部重点实验室，济南 250061

摘 要：为了精确识别金属板料的极限应变并提高成形极限预测精度，建立了一种新的耦合 GTN 模型的三维 M-K 模型，并命名为三维 M-K-GTN 模型。首先，通过引入摩擦应力和沿厚度方向上的法向应力，对经典 M-K 模型进行修正以使其适用于三维应力状态。随后，嵌入 GTN 模型以取代经验失效准则，将凹槽内孔洞体积分数累积到临界值时的应变作为极限应变。此外，考虑法向应力和摩擦应力，修正了孔洞形核与长大表达式。最后，预测成形极限曲线与实验获得的 AA6016-T4 板料极限应变的对比结果表明，三维 M-K-GTN 模型解决了大应变路径下预测结果明显高估的问题，且在每个给定的应变路径下都具有较高的预测精度。

关键词：极限应变识别；孔洞演化；失效准则；三维 M-K-GTN 模型；预测精度

(Edited by Bing YANG)